Published as:
Frost, Ray and Martens, Wayde and Erickson, Kristy (2005) Thermal decomposition of the hydrotalcite Zn6Al2CO3(OH)16.4H2O – a Thermogravimetric analysis and hot stage Raman spectroscopic study. *Journal of Thermal Analysis and Calorimetry* 82(3):pp. 603-608.

Thermal decomposition of the hydrotalcite $Zn_6Al_2CO_3(OH)_{16}.4H_2O$ – a Thermogravimetric analysis and hot stage Raman spectroscopic study

Ray L. Frost•, Wayde N. Martens and Kristy L. Erickson

Inorganic Materials Research Program, School of Physical and Chemical Sciences, Queensland University of Technology, GPO Box 2434, Brisbane Queensland 4001, Australia.

Abstract

A combination of thermogravimetry and hot stage Raman spectroscopy has been used to study the thermal decomposition of the synthesised zinc substituted takovite $Zn_6Al_2CO_3(OH)_{16}.4H_2O$. Thermogravimetry reveals seven mass loss steps at 52, 135, 174, 237, 265, 590 and ~780 °C. MS shows that the first two mass loss steps are due to dehydration, the next two to dehydroxylation, the mass loss step at 265 °C to combined dehydroxylation and decarbonation. The two higher mass loss steps are

• Author to whom correspondence should be addressed (r.frost@qut.edu.au)

attributed to decarbonation. Raman spectra of the hydroxyl stretching region over the 25 to 200 °C temperature range, enable identification of bands attributed to water stretching vibrations, MOH stretching modes and strongly hydrogen bonded CO_3^{2-} - water bands. CO_3^{2-} symmetric stretching modes are observed at 1077 and 1060 cm^{-1}. One possible model is that the band at 1077 cm^{-1} is ascribed to the CO_3^{2-} units bonded to one OH unit and the band at 1092 cm^{-1} is due to the CO_3^{2-} units bonded to two OH units from the Zn-takovite surface. Thermogravimetric analysis when combined with hot stage Raman spectroscopy forms a very powerful technique for the study of the thermal decomposition of minerals such as hydrotalcites.

Keywords: stitchtite, iowaite, desautelsite, takovite, hydrotalcite, Raman spectroscopy, thermal analysis, thermogravimetry

Introduction

Hydrotalcites are natural minerals based upon a brucite structure in which the divalent cation (Mg^{2+}) is replaced with a trivalent cation such as Al^{3+}. This results in a positive surface charge on the brucite-like surface [1-3]. This positive charge must be counterbalanced by negative charges of anions such as CO_3^{2-} or $(SO_4)^{2-}$. This structural arrangement results in the formation of clay-like layers. Hydrotalcites are often termed layered double hydroxides or LDH's. Hydrotalcites are given by the general formula $[M^{2+}_{1-x}M^{3+}_{x}(OH)_2][A^{n-}]_{x/n}.yH_2O$, where M^{2+} and M^{3+} are the di- and trivalent cations in the octahedral positions within the hydroxide layers with x normally between 0.17 and 0.33 [4, 5]. A^{n-} is an exchangeable interlayer anion. In the hydrotalcites reevesite and pyroaurite, the divalent cations are Ni^{2+} and

Mg^{2+} respectively with the trivalent cation being Fe^{3+}. In these cases the carbonate anion is the major interlayer counter anion. These hydrotalcites are based upon the incorporation of carbonate into the interlayer with expansions of around 8 Å. Normally the hydrotalcite structure based upon takovite (Ni,Al) and hydrotalcite (Mg,Al) has basal spacings of ~8.0 Å where the interlayer anion is carbonate. If the carbonate is replaced by sulphate then the mineral carrboydite is obtained. Similarly reevesite is the Ni,Fe hydrotalcite with carbonate as the interlayer anion, which when replaced by sulphate the minerals honessite and hydrohonessite are obtained. If the carbonate is replaced with chloride the mineral iowaite is formed.

Hydrotalcites are important for a number of reasons least of which is as catalysts. As such the thermal stability of the hydrotalcite is important. The potential application of hydrotalcites as catalysts rests with the ability to make mixed metal oxides at the atomic level rather than at a particle level [6, 7]. Such mixed metal oxides are formed through the thermal decomposition of the hydrotalcite [8, 9]. Recently thermal studies when combined with hot stage infrared or Raman spectroscopy has enabled a better understanding of the thermal decomposition of complex mineral systems [10-15]. In this work we report the thermal decomposition of a Zn-substituted takovite using a combination of thermogravimetric analysis coupled to a mass spectrometer and hot stage Raman spectroscopy.

Experimental

Synthetic Minerals

Synthetic hydrotalcite $Zn_6Al_2CO_3(OH)_{16}.4H_2O$ was prepared by the urea method [16]. A solution was prepared containing 0.165M Al^{3+} (as $AlCl_3.6H_2O$) and 0.335M Zn^{2+} (as $ZnCl_2.6H_2O$). To this solution, 1.65M of urea ($CO(NH_2)_2$) was added, and dissolved. The solution was heated to 363K for 24 hours, then filtered and washed several times. The composition of the hydrotalcites was checked by electron probe analyses. The phase composition was checked by X-ray diffraction.

Thermal Analysis

Thermal decomposition of the hydrotalcite was carried out in a TA® Instruments incorporated high-resolution thermogravimetric analyzer (series Q500) in a flowing nitrogen atmosphere (80 cm^3/min). Approximately 50mg of undiluted sample was heated in an open platinum crucible at a rate of 2.0 °C/min up to 500°C. The Heating program of the instrument was regulated precisely to provide a uniform rate of decomposition in the main decomposition stage. The TG instrument was coupled to a Balzers (Pfeiffer) mass spectrometer for gas analysis. Only selected gases were analyzed. The masses corresponding to 16 (O),17 (OH), 18 (H_2O), 28 (CO), 44 (CO_2) were analysed.

Hot Stage Raman Spectroscopy

The crystals of hydrotalcite were placed and orientated on the stage of an Olympus BHSM microscope, equipped with 10x and 50x objectives and part of a Renishaw 1000 Raman microscope system, which also includes a monochromator, a filter system and a Charge Coupled Device (CCD). Raman spectra were excited by a HeNe laser (633 nm) at a resolution of 2 cm^{-1} in the range between 100 and 4000

cm^{-1}. Repeated acquisition using the highest magnification was accumulated to improve the signal to noise ratio. Spectra were calibrated using the 520.5 cm^{-1} line of a silicon wafer. In order to ensure that the correct spectra are obtained, the incident excitation radiation was scrambled. Spectra at elevated temperatures were obtained using a Linkam thermal stage (Scientific Instruments Ltd, Waterfield, Surrey, England). Details of the technique have been published by the authors. [11, 17-19] Spectral manipulation such as baseline adjustment, smoothing and normalisation was performed using the GRAMS® software package (Galactic Industries Corporation, Salem, NH, USA). Band component analysis was undertaken using the Jandel 'Peakfit' software package, which enabled the type of fitting function to be selected and specific parameters to be fixed or varied accordingly. Band fitting was carried out using a Gauss-Lorentz cross-product function with the minimum number of component bands used for the fitting process. The Gauss-Lorentz ratio was maintained at values greater than 0.7 and fitting was undertaken until reproducible results were obtained with squared correlations of r^2 greater than 0.995.

Results and discussion

Thermogravimetric Analysis and Mass spectrometric analysis

The thermogravimetric analysis of the synthetic zinc substituted takovite ($Zn_6Al_2CO_3(OH)_{16}.4H_2O$) is shown in Figure 1. Seven mass loss steps are observed at 52, 135, 174, 237, 265, 590 and ~780 °C. The relative ion current together with the

dtg curve is shown in Figure 2. The ion currents of CO_2 (AMU=44), H_2O (18 & 17) and O_2 (16) are shown. The first two mass loss steps at 52 and 135 °C correspond with the loss of water. The mass losses are 2.7 and 8.1 % respectively. By using the formula for the synthesised zinc takovite the theoretical mass loss of water is 8.467 %. This value appears to correspond with the second mass loss. Thus the first mass loss is attributed to adsorbed water and the second to the interlayer water. In the ion current patterns for H_2O water vapour evolution is observed at 47 and 135 °C.

Thus the chemical reaction is given by:

Mass loss step 1: (desorption of water)

$Zn_6Al_2CO_3(OH)_{16}.xH_2O \rightarrow Zn_6Al_2CO_3(OH)_{16}.4H_2O + (x-4)H_2O$ ---------- (1)

Mass loss step 2: (dehydration)

$Zn_6Al_2CO_3(OH)_{16}.4H_2O \rightarrow Zn_6Al_2CO_3(OH)_{16} + 4H_2O$ ---------- (2)

The two mass loss steps at 174 and 237 °C are assigned to the dehydroxylation of the hydrotalcite. The ion current for evolved water vapour shows two maxima at 171 and 229 °C. It is noted some CO_2 evolution is observed at 229 °C but the CO_2 evolution reaches a maximum at 266 °C. The theoretical mass loss per mole of water is ~2.0 %. Thus the loss of 2.1 % at 174 °C represents a loss of one mole of water per formula unit.

Mass loss step 3 at 174 °C is given by:

$Zn_6Al_2CO_3(OH)_{16} \rightarrow Zn_6OAl_2CO_3(OH)_{14} + H_2O$ ---------- (3)

Mass loss step 4 and 5 at 237 and 265 °C is given by:

$Zn_6OAl_2CO_3(OH)_{14} \rightarrow Zn_6O_8Al_2CO_3 + 7H_2O$ ---------- (4)

and

$Zn_6O_8Al_2CO_3 \rightarrow (ZnO)_6Al_2O_3 + CO_2$ ----------(4)

X-ray diffraction of the decomposition products shows a mixture of Zn and Al oxides. The two higher temperature mass loss steps at 590 and ~780 °C are attributed to the loss of oxygen. The 44 ion current does show some mass gain of evolved CO_2 at these temperatures.

Hot stage Raman spectroscopy

Only a very limited number of Raman studies have been reported so far on the interlayer carbonate anion in hydrotalcites. Takovite is an example of a naturally occurring hydrotalcite with carbonate as the interlayer anion. The spectra of takovite may be compared with that of the synthesised Zn substituted takovite. When the carbonate species is present as a free ion not involved in any bonding it will exhibit a space group of D_{3h}. In the Raman spectrum one will observe ν_1(A'1), ν_3(E') and ν_4(E'). Because of the symmetry of the carbonate ion, the bending non-planar mode ν_2(A"2), the anti-symmetrical stretching mode ν_3(E') and the angle-bending mode ν_4(E'), will occur in the infrared spectrum; these vibrations are expected at around 880, 1415 and 680 cm^{-1}. By contrast, the symmetric stretching mode ν_1(A'1) is infrared inactive. However, changes can be expected when the carbonate ion is intercalated in the hydrotalcite structure as it will be affected by interactions.

The Raman spectra of the 2700 to 3700 cm^{-1} region of the zinc substituted takovite at 25, 50, 100, 150 and 200 °C are shown in Figure 3. A number of features of this suite of spectra may be observed. Firstly the spectra at 25 and 50 °C are similar. Five bands are observed in the hydroxyl stretching region in the 25 °C spectrum at 3595, 3564, 3477, 3392 and 3272 cm^{-1}. Bands are observed in similar positions in the 50 °C spectrum. An additional band of low intensity is observed at 2973 cm^{-1}. This band is found in the 50 °C spectrum at 2931 cm^{-1} and in the 100 and 150 °C spectra at 2912 cm^{-1}. This band is attributed to the water HOH stretching vibration of water hydrogen bonded to the carbonate anion. The intensity of the band increases up to 150 °C but no intensity remains in the 200 °C spectrum. In the 100 °C spectrum bands are observed at 3667, 3593, 3546, 3423 and 3228 cm^{-1}. In comparison the spectrum at 200 °C is very different. Three intense bands are observed at 200 °C at 3625, 3584 and 3523 cm^{-1}. Bands in these positions are attributed to ZnOH and AlOH stretching vibrations. Bands at lower wavenumbers in the 25 to 150 °C spectra are assigned to water stretching modes. No intensity remains in the OH stretching region at temperatures above 200 °C. Both water and OH units have been lost above this temperature. By observing the spectra of the hydroxyl stretching region over the 25 to 200 °C temperature range, bands attributed to water stretching vibrations, MOH stretching modes and HOH- CO_3^{2-} stretching modes have been identified.

The Raman spectra of the CO_3^{2-} symmetric stretching modes are shown in Figure 4. In the 25 °C spectrum two intense bands are observed at 1077 and 1060 cm^{-1}. The bands are sharp with bandwidths of 15 and 14 cm^{-1}. The relative intensities of the bands are 0.87/2.98 which is 0.29. The possible assignment of these bands is to

the CO_3^{2-} units hydrogen bonded to the interlayer water and to CO_3^{2-} units hydrogen bonded to the surface OH units. The two bands are observed at 1077 and 1059 cm^{-1} in the 50 °C spectrum. The intensity ratio is 1.09/4.55 (=0.239). In the 100 °C spectrum the two bands are observed at 1077 and 1063 cm^{-1} with an intensity ratio of 4.06/1.82 (= 2.23). Thus the band attributed to the CO_3^{2-} units hydrogen bonded to the interlayer water has decreased significantly in intensity whereas the band assigned to CO_3^{2-} units hydrogen bonded to the surface OH units has increased significantly in temperature. At 150 °C no intensity remains in the bands at ~1063 cm^{-1}. Two bands are observed at 1095 and 1076 cm^{-1}. The bands are assigned to CO_3^{2-} units hydrogen bonded to the surface OH units. In the 200 °C spectrum two bands are observed at 1092 and 1076 cm^{-1}. One possible model is that the band at 1076 cm^{-1} is ascribed to the CO_3^{2-} units bonded to one OH unit and the band at 1092 cm^{-1} is due to the CO_3^{2-} units bonded to two OH units from the Zn-takovite surface. As the temperature is increased and some hydroxyls are lost the CO_3^{2-} units are forced to bond to more than one OH unit. The observation of a band at the higher wavenumber of 1092 cm^{-1} compared with 1076 cm^{-1} is an indication that the hydrogen bonding is significantly stronger.

No bands in the Raman spectra are observed at around 1350 cm^{-1} which would be attributed to the antisymmetric stretching vibrations. The infrared spectrum of takovite shows two bands at 1351 and 1417 cm^{-1}. These frequencies may be compared with those of aragonite where bands are observed at 1466 and 1464 cm^{-1}; strontiantite at 1450 and 1400 cm^{-1}. As a result of this symmetry lowering the infrared inactive ν_1 mode will be activated. Indeed, a weak band has been observed around 1050-1060 cm^{-1} for the Zn substituted takovite. Two bands are found in the 25

°C spectrum at 1400 and 1368 cm^{-1}. In addition the ν_3 mode shows a small splitting in the order of 32 cm^{-1}. Some papers have only reported the activated ν_1 in combination with a single ν_3 band. In these cases the ν_3 band seems to be broadened due to an overlap of the two split modes ν_3 and ν_{3a}.

The Raman spectra of the Zn-takovite in the 420 to 620 cm^{-1} region is shown in Figure 5. Two distinct sets of bands are observed centred upon ~560 and 475 cm^{-1}. These two spectral profiles are curve resolved into component bands. The data is reported in Table 1. For Zn-takovite a band is observed at 696 cm^{-1} and is attributed to the ν_4 mode. Intensity of this band approaches zero in the 50 °C spectrum and is not observed in the higher temperature spectra. An intense band is observed at 560 cm^{-1} and is attributed to the ν_2 mode. Two low intensity bands are observed at 538 and 494 cm^{-1}. A reasonable explanation for this band was given by Kagunya et al., who showed the presence of a band at 698 and 695 cm^{-1} in the Raman spectra of Mg/Al-hydrotalcites with OH^- and CO_3^{2-} as interlayer anion, respectively and assigned this vibration as the $E_{g(T)}$ mode. A second band is observed in the 25 °C Raman spectrum at 552 cm^{-1} and is also attributed to the ν_2 mode. A third band is observed at 538 cm^{-1}. The intensity ratio of the 560/552/538 cm^{-1} bands is 2.64/1.06/0.6. In the spectrum at 50 °C three bands are observed at 567, 552, 538 cm^{-1} with intensity ratio of 3.68/1.54/1.40. In the spectrum at 100 °C, two bands are observed at 563 and 540 cm^{-1} with an intensity ratio of 1.57/2.07. In the spectra at 150 and 200 °C two bands are found at 572 and 542 cm^{-1}.

In the Raman spectra at 25 °C, three bands are observed at 494, 477 and 447 cm^{-1}. In the 50 °C spectrum the bands are observed at 496, 483 and 448 cm^{-1}. The

band at 483 cm^{-1} has the highest intensity. In the 100 °C spectrum the bands are observed at 489 and 457 cm^{-1} with the first band having the highest intensity. Two bands are observed at 492 and 464 cm^{-1} and shift to 505 and 482 cm^{-1} in the 200 °C spectrum. These bands are attributed to the O-Al-O bending modes. The Raman spectra of the low wavenumber region are shown in Figure 6. Intense bands are observed at 268 cm^{-1} at 25 °C, 260 and 293 cm^{-1} at 50 °C, 267 and 242 cm^{-1} at 100 °C, 265 and 229 cm^{-1} in the 150 °C and 266 and 220 cm^{-1} in the 200 °C spectrum. The attribution of these bands is to Mg-O and Al-O stretching vibrations.

Conclusions

Thermogravimetric analysis coupled to evolved gas mass spectrometry enable two mass loss steps attributed to dehydration and three steps attributed to dehydroxylation to be identified. Three mass losses ascribed to loss of carbonate were observed, one large mass loss step at 265 °C and two minor steps at 590 and ~780 °C. Hot stage Raman spectroscopy enabled bands attributable to three types of hydroxyl stretching vibrations to be identified: (a) OH stretching vibrations assigned to MOH vibrations (b) water OH stretching vibrations and (c) HOH stretching vibrations resulting from water strongly hydrogen bonded to the carbonate anion. Two intense bands in the 25 °C spectrum are observed at 1077 and 1060 cm^{-1} and are assigned to the CO_3^{2-} units hydrogen bonded to the interlayer water and to CO_3^{2-} units hydrogen bonded to the surface OH units. At higher temperatures a band at ~1095 cm^{-1} is observed and is assigned to CO_3^{2-} units hydrogen bonded to more than one surface OH units. In this work we have proposed a model based upon a

combination of thermogravimetry and hot stage Raman spectroscopy for the thermal decomposition of a $Zn_6Al_2CO_3(OH)_{16}.4H_2O$ hydrotalcite.

Acknowledgements

The financial and infra-structure support of the Queensland University of Technology Inorganic Materials Research Program is gratefully acknowledged. The Australian Research Council (ARC) is thanked for funding the Thermal Analysis Facility.

References

1. R. L. Frost, Z. Ding and J. T. Kloprogge, Canadian Journal of Analytical Sciences and Spectroscopy 45 (2000) 96.
2. R. L. Frost, Z. Ding, W. N. Martens, T. E. Johnson and J. T. Kloprogge, Spectrochimica Acta, Part A: Molecular and Biomolecular Spectroscopy 59A (2003) 321.
3. L. Hickey, J. T. Kloprogge and R. L. Frost, Journal of Materials Science 35 (2000) 4347.
4. J. T. Kloprogge, D. Wharton, L. Hickey and R. L. Frost, American Mineralogist 87 (2002) 623.
5. V. Rives and Editor, *Layered Double Hydroxides: Present and Future*, 2001.
6. R. L. Frost and K. L. Erickson, Journal of Thermal Analysis and Calorimetry 76 (2004) 217.
7. R. L. Frost and M. L. Weier, Journal of Thermal Analysis and Calorimetry 75 (2004) 277.
8. F. Rey, V. Fornes and J. M. Rojo, J. Chem. Soc., Faraday Trans. 88 (1992) 2233.
9. M. Valcheva-Traykova, N. Davidova and A. Weiss, J. Mater. Sci. 28 (1993) 2157.
10. R. L. Frost, M. Adebajo and M. L. Weier, Spectrochimica Acta, Part A: Molecular and Biomolecular Spectroscopy 60 (2004) 643.
11. R. L. Frost and M. L. Weier, Thermochimica Acta 409 (2004) 79.
12. R. L. Frost, Z. Ding, W. N. Martens and T. E. Johnson, Thermochimica Acta 398 (2003) 167.
13. R. L. Frost, Z. Ding and H. D. Ruan, Journal of Thermal Analysis and Calorimetry 71 (2003) 783.
14. R. L. Frost, E. Horvath, E. Mako, J. Kristof and A. Redey, Thermochimica Acta 408 (2003) 103.
15. E. Horvath, R. L. Frost, E. Mako, J. Kristof and T. Cseh, Thermochimica Acta 404 (2003) 227.
16. U. Costantino, F. Marmottini, M. Nocchetti and R. Vivani, European Journal of Inorganic Chemistry (1998) 1439.
17. R. L. Frost and M. L. Weier, Thermochimica Acta 406 (2003) 221.
18. R. L. Frost, M. L. Weier and J. T. Kloprogge, Journal of Raman Spectroscopy 34 (2003) 760.
19. R. L. Frost and M. L. Weier, Journal of Raman Spectroscopy 34 (2003) 776.

25°C			50°C			100°C			150°C			200°C		
Band Centre (cm^{-1})	FWHM (cm^{-1})	*Intensity (%)*	**Band Centre (cm^{-1})**	FWHM (cm^{-1})	*Intensity (%)*	**Band Centre (cm^{-1})**	FWHM (cm^{-1})	*Intensity (%)*	**Band Centre (cm^{-1})**	FWHM (cm^{-1})	*Intensity (%)*	**Band Centre (cm^{-1})**	FWHM (cm^{-1})	*Intensity (%)*
3595	47	*2.03*	**3593**	39	*3.93*	**3667**	59	*4.72*	**3601**	134	*15.26*	**3725**	29	*0.55*
3564	132	*11.00*	**3570**	137	*9.41*	**3593**	74	*5.12*	**3590**	48	*1.60*	**3625**	77	*6.84*
3477	130	*21.07*	**3494**	198	*16.68*	**3546**	157	*16.63*	**3519**	189	*16.68*	**3584**	80	*14.48*
3392	168	*22.87*	**3397**	267	*35.65*	**3423**	219	*31.02*	**3364**	290	*33.04*	**3523**	131	*20.27*
3272	301	*24.52*	**3138**	281	*8.65*	**3228**	384	*17.78*	**3093**	250	*10.01*	**3430**	84	*6.41*
2973	235	*3.37*	**2931**	98	*1.23*	**2912**	124	*3.29*	**2912**	110	*4.58*			
1400	28	*0.42*												
1368	14	*0.13*												
1093	16	*0.13*	**1088**	21	*0.40*	**1102**	29	*0.37*	**1095**	45	*2.78*	**1092**	44	*8.10*
1077	15	*0.87*	**1077**	14	*1.09*	**1077**	21	*4.06*	**1076**	28	*6.09*	**1076**	29	*11.88*
1060	14	*2.98*	**1059**	17	*4.55*	**1063**	50	*1.82*	**1047**	30	*0.48*	**1047**	39	*3.33*
1052	18	*0.31*	**1040**	63	*1.26*	**1062**	47	*2.21*						
			956	74	*1.65*	**980**	81	*1.63*						
696	19	*0.11*												
560	58	*2.64*	**567**	51	*3.68*	**563**	39	*1.57*	**572**	32	*0.45*	**572**	39	*1.97*
552	23	*1.06*	**552**	24	*1.54*	**540**	31	*2.07*	**542**	32	*1.47*	**542**	24	*0.99*
538	18	*0.60*	**538**	30	*1.40*									
494	24	*0.96*	**496**	16	*0.32*	**489**	43	*3.41*	**492**	45	*2.37*	**505**	32	*1.14*
477	35	*1.89*	**483**	41	*4.56*	**457**	36	*0.86*	**464**	31	*0.31*	**482**	31	*1.17*
447	24	*0.22*	**448**	31	*0.73*									
388	31	*0.22*	**380**	37	*0.48*	**376**	34	*0.41*	**386**	41	*0.21*	**388**	30	*0.63*
268	52	*1.59*	**293**	41	*0.79*	**267**	47	*1.74*	**265**	50	*4.32*	**266**	68	*18.78*
231	23	*0.40*	**260**	49	*1.95*	**242**	32	*0.32*	**229**	24	*0.35*	**220**	33	*3.47*
212	22	*0.41*	**216**	11	*0.07*									

195 · 13 · *0.18*				

Table 1 Results of the Raman spectra of synthetic zinc substituted takovite at 25, 50, 100, 150 and 200 °C.

List of Figures

Figure 1 TG and DTG of synthetic zinc substituted takovite

Figure 2 MS and DTG of synthetic zinc substituted takovite

Figure 3 Raman spectra of the 2700 to 3700 cm^{-1} region of synthetic zinc substituted takovite

Figure 4 Raman spectra of the 900 to 1200 cm^{-1} region of synthetic zinc substituted takovite

Figure 5 Raman spectra of the 400 to 600 cm^{-1} region of synthetic zinc substituted takovite

Figure 6 Raman spectra of the 175 to 425 cm^{-1} region of synthetic zinc substituted takovite

List of Tables

Table 1 Results of the Raman spectra of synthetic zinc substituted takovite at 25, 50, 100, 150 and 200 °C.

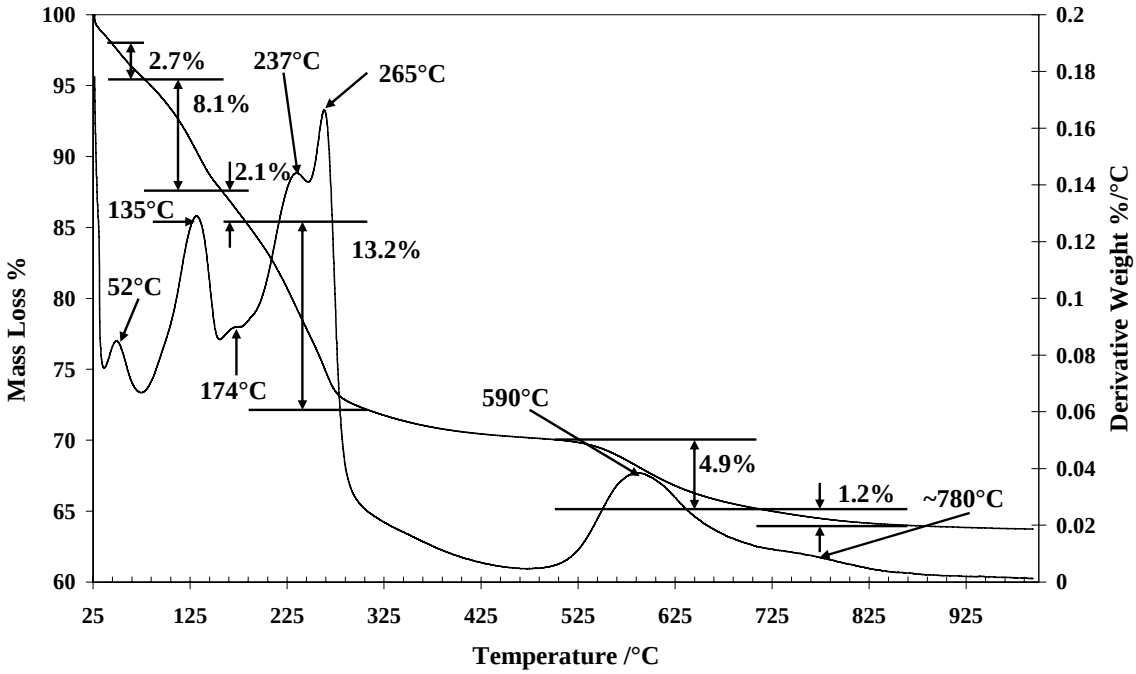
Mass Loss %
Derivative Weight %/°C
Temperature /°C
2.7%
8.1%
2.1%
13.2%
4.9%
1.2%
237°C
265°C
135°C
52°C
174°C
590°C
~780°C

Figure 1

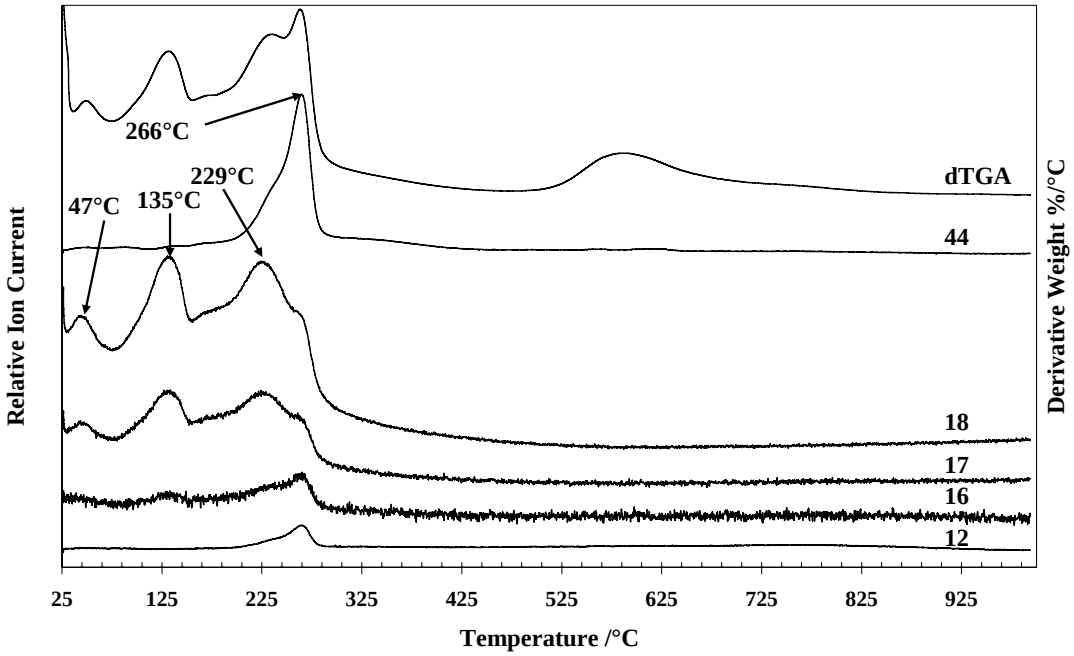
266°C
229°C
47°C
135°C
dTGA
44
18
17
16
12
Relative Ion Current
Derivative Weight %/°C
25
125
225
325
425
525
625
725
825
925
Temperature /°C

Figure 2

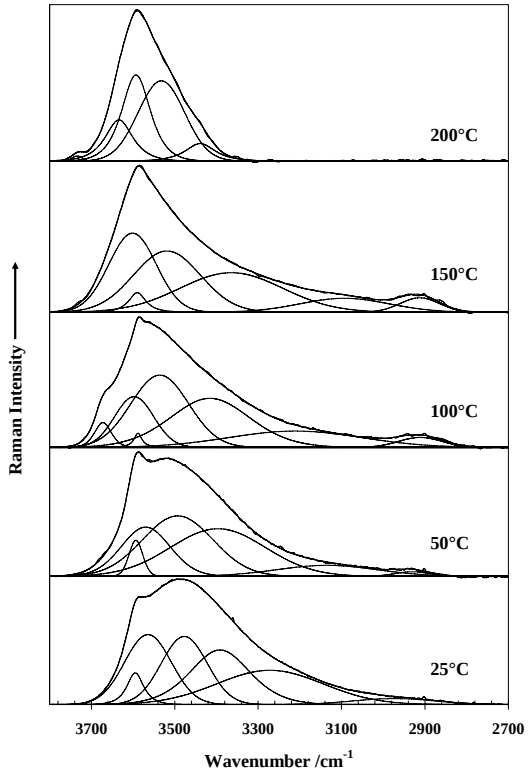
200°C
150°C
100°C
50°C
25°C
Raman Intensity
3700
3500
3300
3100
2900
2700
Wavenumber /cm-1

Figure 3

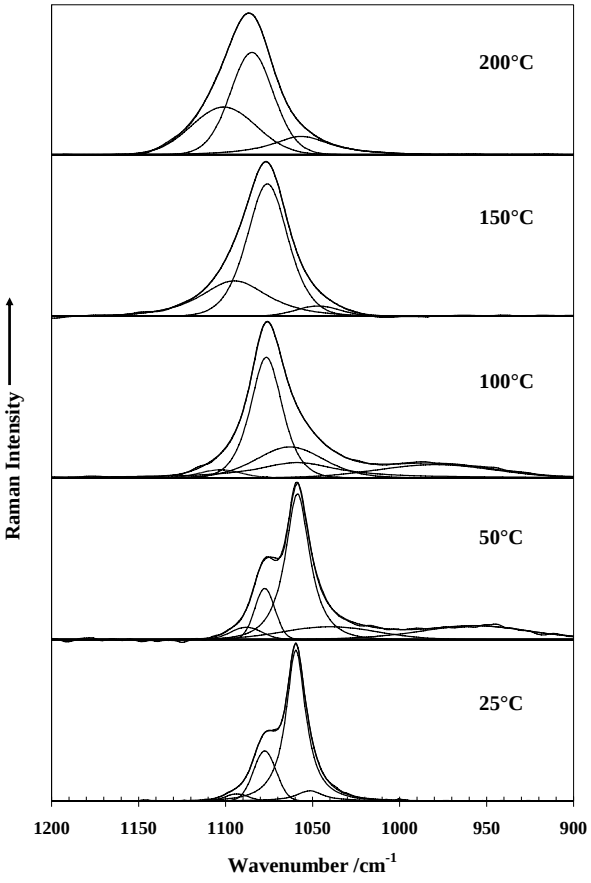
200°C
150°C
100°C
50°C
25°C
Raman Intensity
1200
1150
1100
1050
1000
950
900
Wavenumber /cm-1

Figure 4

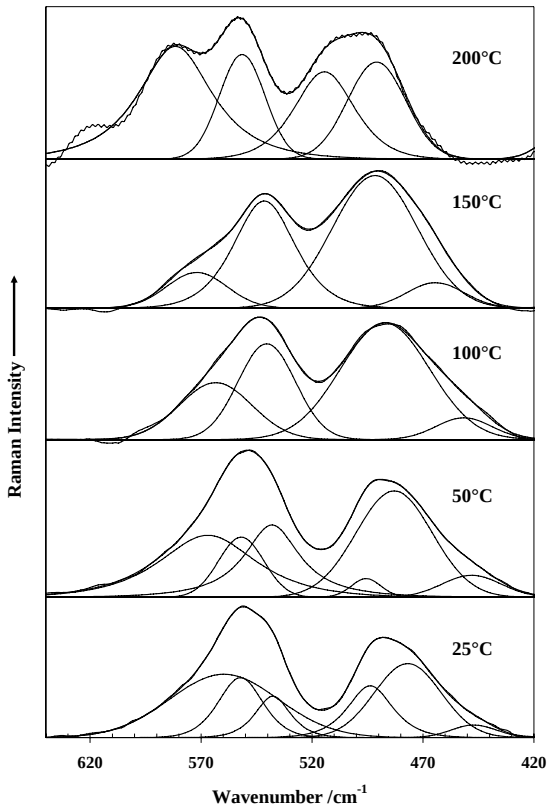
200°C
150°C
100°C
50°C
25°C
Raman Intensity
620
570
520
470
420
Wavenumber /cm-1

Figure 5

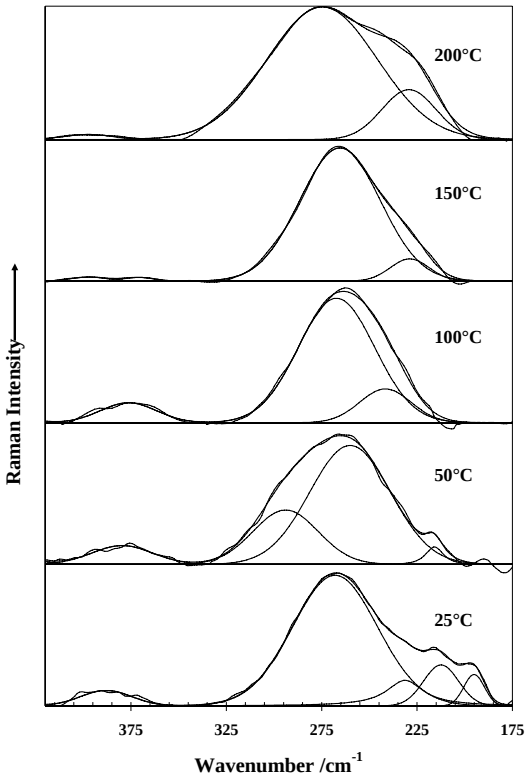
200°C
150°C
100°C
50°C
25°C
Raman Intensity
375
325
275
225
175
Wavenumber /cm-1

Figure 6